ACS OMEGA

Open Access

http://pubs.acs.org/journal/acsodf

Article

Design, Synthesis, and Anti-Breast Cancer Potential of Imidazole−Pyridine Hybrid Molecules *In Vitro* and Ehrlich Ascites Carcinoma Growth Inhibitory Activity Assessment *In Vivo*

Baladhandapani Aruchamy, Mahadevaswamy G. Kuruburu, Venugopal R. Bovilla, SubbaRao V. Madhunapantula, Carmelo Drago,* Sonu Benny, Aneesh Thankappan Presanna, and Prasanna Ramani*

Cite This: *ACS Omega* 2023, 8, 40287−40298

Read Online

ACCESS | Metrics & More | Article Recommendations | Supporting Information

ABSTRACT: Breast cancer remains a challenging medical issue and is a high priority for biomedical research despite significant advancements in cancer research and therapy. The current study aims to determine the anticancer activity of a group of imidazole−pyridine-based scaffolds against a variety of breast cancer cell lines differing in their receptor expression (estrogen receptor (ER), progesterone receptor (PR), and HER-2). A series of 10 molecules (coded **5a**−**5j**) were synthesized through multicomponent and alkylation reactions. FTIR, MS, ^{1}H, and ^{13}C NMR spectral analyses confirmed the structures and purity of the synthesized molecules. Subsequently, these molecules were tested for their ability to inhibit the viability of cell lines representing carcinoma of the breast, viz., MDA-MB-468 (ER−, PR−, and HER−), BT-474 (ER+, PR+, and HER+), T-47D (ER+, PR+, and HER−), and MCF-7 (ER+, PR+, and HER−) in vitro. Among these 10 molecules, **5a**, **5c**, **5d**, and **5e** exhibited better potency, as evidenced by IC_{50} < 50 μM at 24 h of treatment against BT-474 and MDA-MB-468 cell lines. However, except for **5d**, the IC_{50} value is much higher than 50 μM when tested against T47D and MCF-7 cell lines at 24h. Extended treatment for 48 h reduced the effect of these molecules, as an increase in IC_{50} was observed. In mice, intraperitoneal administration of **5e** retarded the Ehrlich ascites carcinoma (EAC) growth without causing any organ toxicity at the doses tested. In summary, we report the synthesis scheme and key structural requirements for a new series of imidazole−pyridine molecules for *in vitro* inhibition of the feasibility of breast cancer cells and *in vivo* inhibition of EAC tumors.

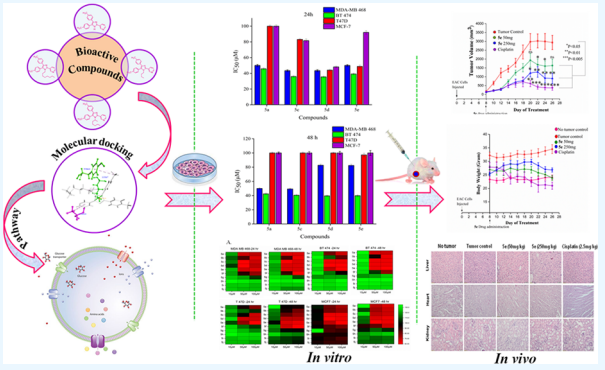

1. INTRODUCTION

Among women worldwide, breast cancer is the second most significant contributor to cancer-related fatalities, following lung cancer.[1] Depending on the size of the tumor, cancer stage, aggressiveness, grade, metastatic behavior, intrinsic molecular subtyping of the tumor, age, menopausal status, comorbidities, general health, and preferences of the patient, clinicians have the options to choose from a variety of medicines to treat breast cancer.[2,3] Patient survival rates have been substantially enhanced by a comprehensive range of highly efficacious breast cancer treatments, including targeted therapy, immunotherapy, chemotherapy, radiation therapy, and surgery.[4−6] Chemotherapy, in which various anticancer drugs are used to treat tumor cells, has become a crucial component in cancer treatment.[7] For the treatment of breast cancer, the current therapeutic protocols involve the administration of adjuvant medications, which encompass anthracyclines (such as doxorubicin and epirubicin), taxanes (like paclitaxel and docetaxel), as well as fluorouracil and cyclophosphamide.[8,9]

The classification of breast cancers is determined by the expression levels of the specific receptors mentioned, including PR (progesterone receptor), ER (estrogen receptor), and HER-2 (human epithelial receptor 2). Most of the breast cancer cases, exceeding 75%, exhibit a positive hormone receptor status. However, there is limited availability of effective treatment options specifically tailored for these subtypes.[10,11] Therefore, developing more effective and less toxic chemotherapeutic agents is an immediate requirement.

Imidazole and its derivatives are the most prevalent versatile units of heterocyclic chemistry, and they possess outstanding pharmaceutical activities to control cancer.[12−16] Clinical trials

Received: June 20, 2023
Accepted: September 15, 2023
Published: October 19, 2023

have evaluated the efficacy of various imidazole-containing drugs, including dacarbazine, temozolomide, etanidazole, azathioprine, zoledronic acid, pimonidazole, misonidazole, mercaptopurine, nilotinib, fadrozole, and tipifarnib, in the treatment of various types of cancer, with the current availability for clinical use.[14,17] Recently, our research efforts have focused on conducting comprehensive studies aimed at developing highly potent anticancer agents. There are numerous scientific studies available which employ innovative and novel synthetic methods to synthesize 2,4,5 tri- and 1,2,4,5 tetra-substituted imidazole heterocyclic compounds.[18−21] New hybrid molecules with potent biological activities are produced by the molecular hybridization approach, involving two or more biologically active pharmacophores.[22−25] The combination of these two significant moieties could lead to possible imidazole−pyridine hybrid molecules with enhanced biological activities.[26−31] The introduction of the hetero unit on position 2 of the imidazole scaffold exhibits potential anticancer activity.[32] In addition, the phenyl rings present at positions 4 and 5 are increasingly crucial for the cytotoxicity of the imidazole moiety when compared to aliphatic substitution on these positions.[14] As part of this study, we devised and created a new category of 3-(4,5-ditolyl-1H-imidazol-2-yl) pyridine derivatives using our novel design and synthesis methods (Figure 1) with promising *in vivo* and *in vitro* efficacy and the potential to consider as the next generation of molecules for better breast cancer treatment.

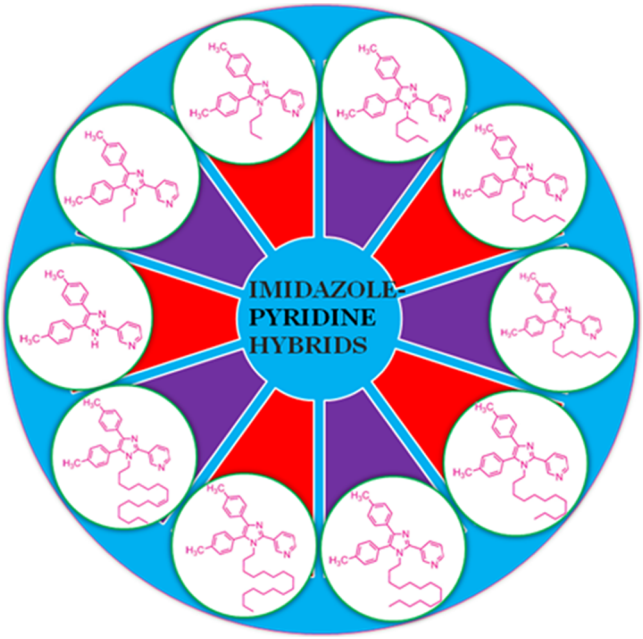

Figure 1. Imidazole−pyridine hybrid molecules.

2. RESULTS AND DISCUSSION

2.1. Synthesis. The imidazole−pyridine compound **5a** was synthesized as per Scheme 1.[26,33] To prepare the desired compound, pyridine-3-carboxaldehyde, 4,4′-dimethylbenzil, and ammonium acetate were dissolved in ethanol. The resulting solution was then subjected to reflux for 12 h, utilizing a catalytic amount of iodine. The reaction was terminated, and the mixture was further processed upon the disappearance of pyridine-3-carboxaldehyde, as observed

Scheme 1. Synthetic Pathways for the Target Imidazole−Pyridine Scaffold[a]

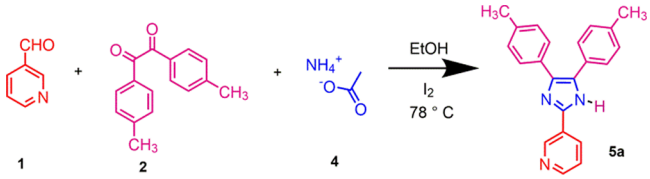

[a]Reagents and conditions; absolute EtOH/I_2, 78 °C, 12 h.

through thin-layer chromatography (TLC). After the column chromatography purification technique was employed, a 2,4,5-tri-substituted imidazole compound with a high purity yield of 72% was obtained. The reaction was performed using various primary amines to reach the desired compounds (Scheme 2). A primary amine, 4,4′-dimethylbenzil, pyridine-3-carboxaldehyde, and ammonium acetate were dissolved in ethanol to create **5c−5e** and **5j** in good yields (56−72%).

Scheme 2. Synthetic Pathways for the Target Imidazole−Pyridine Scaffold[a]

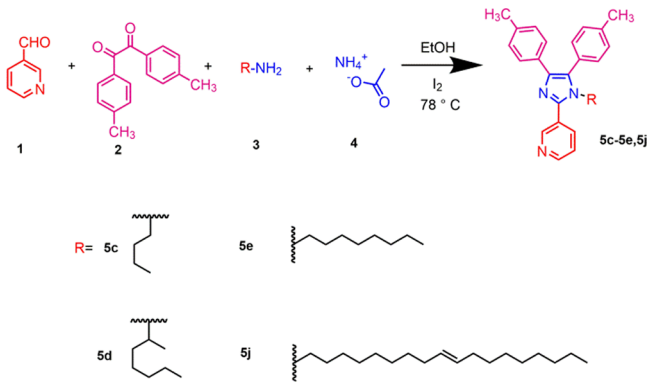

[a]Reagents and conditions; absolute EtOH/I_2, 78 °C, 8−15h.

The structure of all molecules was confirmed by MS, FTIR, and NMR spectra (^{1}H and ^{13}C NMR). During the ESI-MS analysis, the target compounds exhibited prominent peaks corresponding to the [M^+] ions. Distinctive absorption bands were observed in the FTIR spectrum of the target compound **5a**. Notably, an absorption peak at 3742 cm^{-1} indicated the presence of N−H stretching, while the C−H stretching frequency of the aromatic structure appeared at 3064 cm^{-1}. The observed bands at 1695 and 1519 cm^{-1} in the spectrum are attributed to the C═N and C═C bonds, respectively. In addition, the band at 1021 cm^{-1} is due to the C−N group. On the other hand, aromatic protons appeared as multiplets in the ^{1}H NMR spectrum of **5a** at δ 7.12−7.42. Pyridine ring hydrogens (3H) appeared as singlet and doublet between δ 8.40 and 9.05 ppm. The ^{13}C NMR spectra for this compound showed signals of pyridine ring at δ 148.83, 145.84, and 142.75 and aromatic ring at 136.91, 133.41, 129.29, 127.80, 126.77, and 123.92 ppm, which further confirm the structure. A methyl group is present at 21.27 ppm. In the mass spectrum, the [M^+] ion peak of compound **5a** was detected at m/z = 325.10, congruent with the molecular formula $C_{22}H_{19}N_3$. In the FTIR spectrum of active compound **5d**, distinct absorption bands were observed, indicating specific chemical functionalities. Notably, an absorption peak at 3246 cm^{-1} corresponded to the

https://doi.org/10.1021/acsomega.3c04384
ACS Omega 2023, 8, 40287−40298

stretching vibrations of the aromatic ring. The bands at 2917 and 2849 cm^{-1} were assigned to the C−H stretching vibrations of the aliphatic chain in the attached imidazole ring at the first position. Additionally, the bands at 1432, 1609, and 1021 cm^{-1} were assigned to the vibrations of the C═C, C═N, and C−N bonds, respectively. In the ^{1}H NMR spectrum of compound **5d**, characteristic signals were observed for different proton environments. A triplet was observed in the range of δ 0.77−0.80 ppm, which can be assigned to the CH_3 protons. Additionally, multiplets in the range of δ 4.13−4.20 ppm were indicative of the CH protons in the aliphatic chain. The aromatic protons were observed as multiplets in the range of δ 6.97−7.96 ppm. Pyridine ring hydrogens appeared at δ 8.68−8.84 ppm, respectively. The ^{13}C NMR spectrum of compound **5d** exhibited distinctive signals corresponding to aliphatic and aromatic carbons. Aliphatic signals were observed at δ 13.96, 21.11, 21.46, 22.41, 26.04, 29.70, 31.22, 36.15, 53.97, and 64.39 ppm. Aromatic signals were observed at δ 123.26, 126.51, 128.75, 128.95, 129.53, 131.55, 137.62, and 138.85 ppm. Additionally, two signals for singlet protons at δ 149.79 and 150.47 ppm were assigned to the pyridine ring moiety, further confirming the structure. In the mass spectrum, the [M^+] ion peak of the active compound **5d** was detected at m/z = 423 (M^+), consistent with the molecular formula $C_{29}H_{33}N_3$. This agreement provides further confirmation of the compound's molecular composition.

The alkylation reaction of (4,5-ditolyl-1H-imidazol-2-yl) pyridine (**5a**) was carried out in acetonitrile and anhydrous K_2CO_3 to generate *N*-alkylated (**5b**, **5f**−**5i**) imidazole−pyridine scaffold, respectively (Scheme 3). The progression

Scheme 3. *N*-Alkylation Reactions

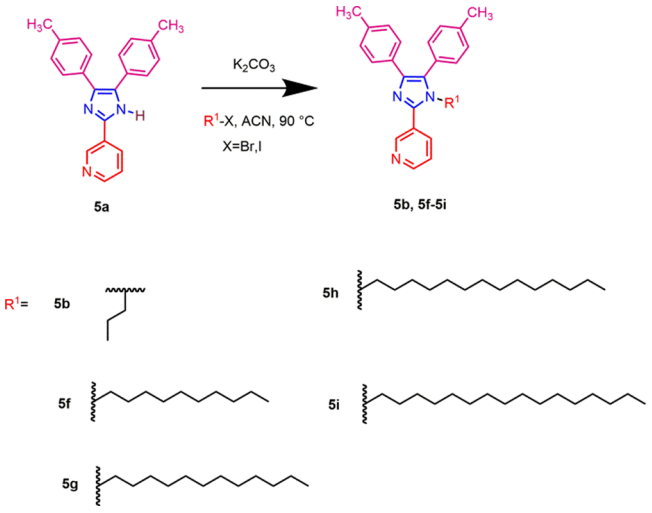

of the reaction was tracked using thin-layer chromatography (TLC), and the appearance of new spots in the chromatogram determined the completion. The product was obtained at a yield of 56−64%. The structure of compounds (**5b**) and (**5f**−**5i**) was determined from their spectral analyses, NMR, FTIR, and MS spectra, which agreed with the assigned structures (refer to Section 5). A plausible mechanism for the synthesis of tri-substituted imidazoles is presented in Scheme 4.[34]

2.2. Biological Evaluation. *2.2.1. In Vitro Evaluation of Biological Activity.* Based on the inhibition results, we further investigated the cytotoxicity activity of the compounds in MCF-7, BT474, T47D, and MDA-MB-468 as well as normal

Scheme 4. Probable Mechanism

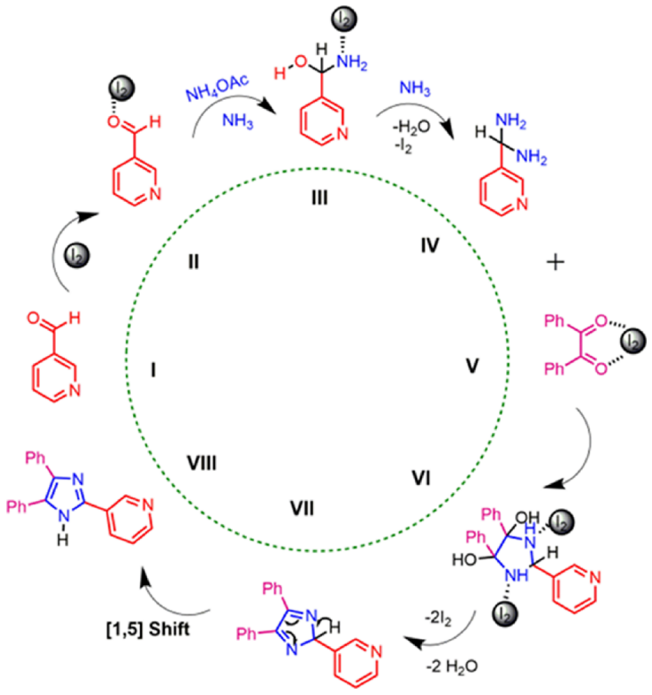

cell lines L929 (mouse fibroblast cells) using a sulforhodamine-B (SRB) assay (heat map in Figure 2A). Cisplatin was used as a reference drug. In Table 1, it is observed that compounds **5a**−**5j** exhibited potent inhibitory activity against all target cell lines. Notably, compounds **5a**, **5c**, **5d**, and **5e** demonstrated higher levels of potency compared to the other compounds in the study (Figure 2B). In particular, the more potent cytotoxicity activity of **5e** (IC_{50} = 39.19 ± 1.12 μM at 24 h and 39.85 ± 1.25 μM at 48 h) was shown against the BT474 cell line. On the other hand, **5c** (IC_{50} = 35.98 ± 1.09 μM at 24 h and 40.47 ± 1.13 μM at 48 h) and **5d** (IC_{50} = 35.56 ± 1.02 μM at 24 h and 39.62 ± 1.09 μM at 48 h) showed high activity against the BT474 cell line.

The IC_{50} value of compound **5a** (IC_{50} = 45.82 ± 1.32 μM at 24 h and 42.40 ± 1.21 μM at 48 h) without alkyl substitution in the N1 position of imidazole ring is slightly high compared to that of the alkyl-substituted compounds **5c**, **5d,** and **5e**. Moreover, we assessed the cytotoxicity of compounds **5a**, **5c**, **5d**, and **5e** against the MDA-MB468 cell line at both 24 and 48 h intervals. The results showed that compound **5c** (IC_{50} = 43.46 ± 1.08 μM at 24 h and 49.23 ± 1.21 μM at 48 h) possessed elevated activity compared to the other compounds in the study. Based on these results, it can be surmised that there is a favorable reduction in the IC_{50} value with an increase in the alkyl chain length at the N1 nitrogen of the imidazole ring (>100 μM). Subsequently, to determine IC_{50} and evaluate their safety, the cytotoxicity of the active compounds **5a**, **5c**, **5d,** and **5e** was tested against the normal cell line L929 (mouse fibroblast cells) in Table 1. All the active compounds exhibited varying levels of cytotoxic activity against the L929 cell line, with IC_{50} values in the range of 88.41 ± 1.08 and 48.12 ± 1.17 μM. Specifically, the IC_{50} values for the compounds were 88.41 ± 1.08, 48.12 ± 1.17, 57.24 ± 1.05, and 67.24 ± 1.12 μM. The results indicated that **5e** displayed more potent cytotoxic activity in the BT474 cell line.

A similar investigation was conducted on **5a′** and **5e′** (Figure 3) to check the influence of methyl functionality

https://doi.org/10.1021/acsomega.3c04384
ACS Omega 2023, 8, 40287−40298

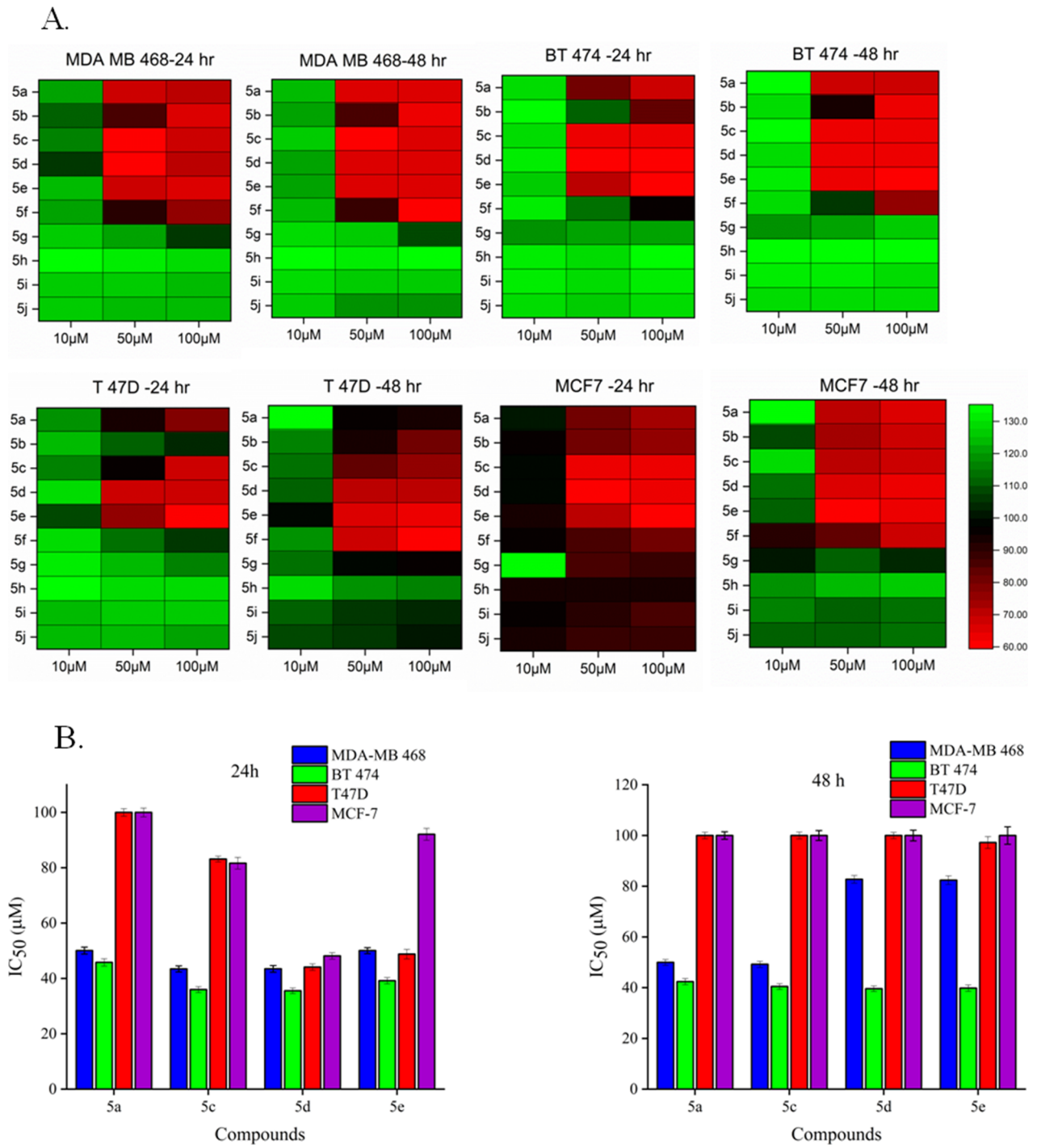

Figure 2. (A) Heat map based on the percentage of inhibition induced by every compound at different concentrations for 24 and 48 h. (B) IC_{50} values of compounds/analogues **5a**, **5c**, **5d,** and **5e** against four breast cancer cell lines.

against the chosen cell lines. The IC_{50} values of **5a′** were calculated for both 24 and 48 h and were found to be 94.64 ± 1.32 and 62.68 ± 1.09 μM for MDA-MB-468; 92.51 ± 1.71 and 57.59 ± 1.65 μM for BT 474, greater than 100 μM for both T47D and MCF-7. Compound **5e′** exhibited IC_{50} values of 67.04 ± 1.43 and 87.17 ± 1.27 μM against the MDA-MB 468 cell line, 29.16 ± 2.1 and 53.22 ± 1.91 μM against the BT 474 cell line, 65.75 ± 1.53 μM and >100 μM against the T47D cell line, and 82.56 ± 1.21 and >100 μM against the MCF-7 cell line. These results reflect that substituting a methyl group on the para position proved to be potent against breast cancer cell lines in comparison with the unsubstituted molecules.

*2.2.2. In Vivo Antitumor Efficacy of **5e**.* A mouse model bearing Ehrlich Ascites Carcinoma (EAC) cells was used to evaluate the therapeutic efficacy of **5e** (Figure 4). The positive control, 2.5 mg/kg cisplatin, and test compound **5e** were administered every alternate day for a period of 26 days. Compound **5e** was known at dosages of 50 and 250 mg/kg, and cisplatin as the positive control was administered at an intraperitoneal dose of 2.5 mg/kg. Retardation in tumor growth was observed in the case of cisplatin and compound **5e**

https://doi.org/10.1021/acsomega.3c04384
ACS Omega 2023, 8, 40287−40298

Table 1. *In Vitro* Cytotoxicity of 5a−5j on Various Breast Cancer Cell Lines at 24 and 48 h

	mouse fibroblast cell line IC_{50}[a] ± SD (μM)	breast cancer cell lines [IC_{50}[a] ± SD (μM)]							
		MDA-MB 468		BT 474		T47D		MCF-7	
code	L929	24h	48h	24h	48h	24h	48h	24h	48h
5a	88.41 ± 1.08	**50.08 ± 1.24**	**49.98 ± 1.13**	45.82 ± 1.32	**42.40 ± 1.21**	>100 μM	>100 μM	>100 μM	>100 μM
5b	26.59 ± 1.32	97.88 ± 1.36	100.21 ± 1.69	97.10 ± 1.21	72.48 ± 1.46	>100 μM	>100 μM	>100 μM	>100 μM
5c	48.12 ± 1.17	43.46 ± 1.08	**49.23 ± 1.21**	**35.98 ± 1.09**	40.47 ± 1.13	83.16 ± 1.04	>100 μM	81.66 ± 2.13	>100 μM
5d	57.24 ± 1.05	**43.48 ± 1.19**	82.75 ± 1.5	**35.56 ± 1.02**	**39.62 ± 1.09**	44.11 ± 1.16	>100 μM	**48.15 ± 1.19**	>100 μM
5e	67.24 ± 1.12	**50.08 ± 1.07**	82.39 ± 1.69	**39.19 ± 1.12**	**39.85 ± 1.25**	**48.8 ± 1.72**	97.24 ± 2.34	92.11 ± 2.14	>100 μM
5f	198.8 ± 1.85	>100 μM	94.47 ± 2.36	>100 μM	92.97 ± 1.95	>100 μM	90.61 ± 3.2	>100 μM	>100 μM
5g	283.79 ± 2.13	>100 μM	>100 μM	>100 μM	>100 μM	>100 μM	>100 μM	>100 μM	>100 μM
5h	346.62 ± 1.51	>100 μM	>100 μM	>100 μM	>100 μM	>100 μM	>100 μM	>100 μM	>100 μM
5i	409.37 ± 1.39	>100 μM	>100 μM	>100 μM	>100 μM	>100 μM	>100 μM	>100 μM	>100 μM
5j	87.61 ± 1.62	>100 μM	>100 μM	>100 μM	>100 μM	>100 μM	>100 μM	>100 μM	>100 μM
5a′	83.79 ± 1.76	94.64 ± 1.32	62.68 ± 1.09	92.51 ± 1.71	57.59 ± 1.65	>100 μM	>100 μM	>100 μM	>100 μM
5e′	61.70 ± 1.91	67.04 ± 1.43	87.17 ± 1.27	29.16 ± 2.1	53.22 ± 1.91	65.75 ± 1.53	>100 μM	82.56 ± 1.21	>100 μM

[a]IC_{50}: concentration that inhibits 50% of cell growth. Mean ± SD of at least three independent experiments. SRB assay was used to determine the IC_{50} values.

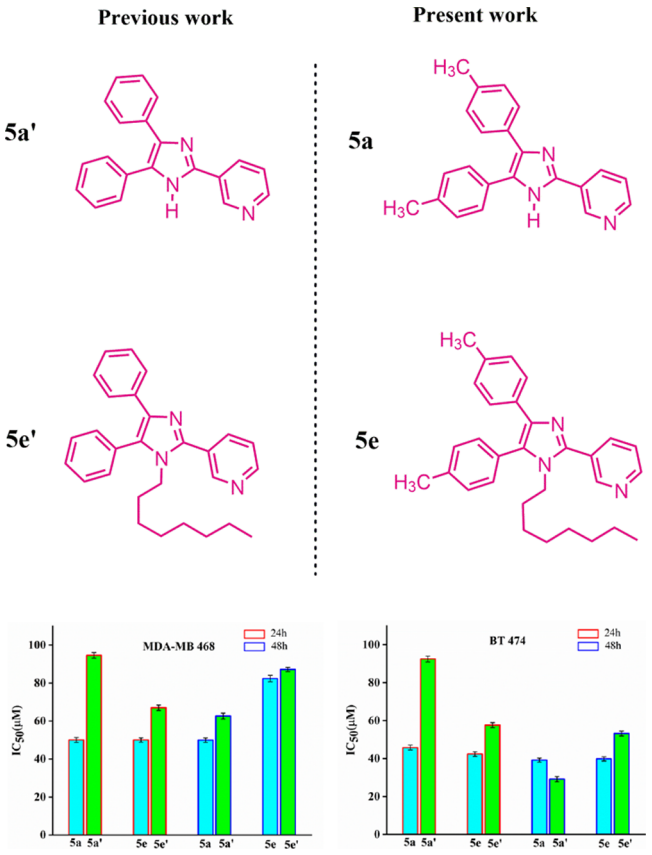

Figure 3. Representative 2,4,5-tri-substituted and 1,2,4,5-tetra-substituted imidazole scaffolds, with a different substitution mode.

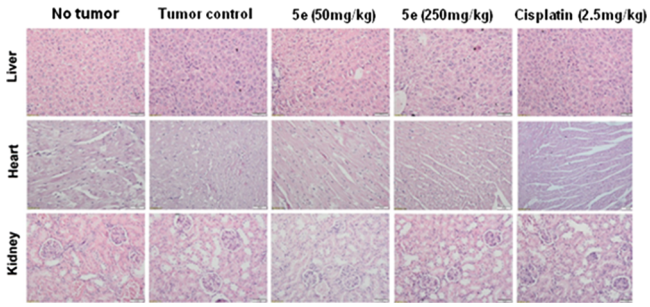

Figure 4. H&E staining of vital organs showed no significant changes in the morphology and tissue architecture upon treatment with **5e**.

in this mouse model. A notable decrease in tumor volume was observed starting from day 6 of the drug treatment, indicating the effectiveness of the treatment in inhibiting tumor growth (Figure 5A). By the end of the experiment, specifically on day 26, a substantial diminution was observed in the tumor size. With the administration of 50 mg/kg dose, approximately 50% diminution in tumor size was observed. Furthermore, administering a 250 mg/kg dose reduced the tumor size by approximately 66% (Figure 5A). Under these experimental conditions, the experimental mice body weight and vital organ morphology have not changed during the treatment (Figure 5B). In summary, compound **5e** retarded the EAC growth without causing organ damage.

2.3. Molecular Modeling Studies. Molecular docking is an important computational method of finding new drug candidates by analyzing their binding affinity toward particular receptors.[35,36] The crystal structures of selected target proteins were collected from the Protein Databank (PDB ID: 4KZN for VEGF, 7NH5 for Akt, 5W9C for ER, 3QYC for HER-2, and

https://doi.org/10.1021/acsomega.3c04384
ACS Omega 2023, 8, 40287−40298

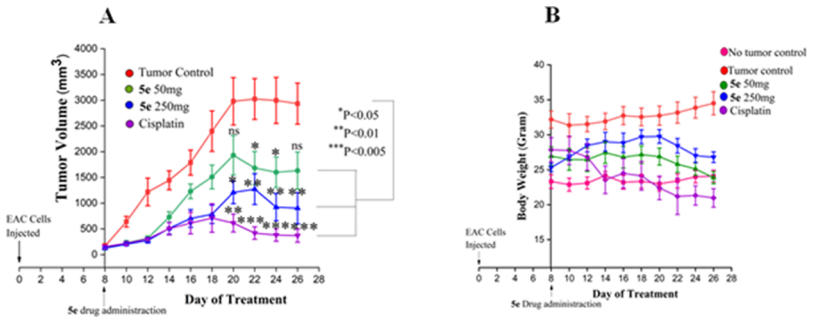

Figure 5. Graphical illustration of the changes in tumor volume (A) and body weight (B) for **5e** and cisplatin.

5GPG for mTOR). The active sites or binding pockets of the targets were identified through a cocrystallized ligand for the corresponding protein or via literature review. The docking scores provide information about the binding affinity of the molecule, indicating how strongly it interacts with the target protein. On the other hand, the amino acid interaction networks illustrate the specific protein−ligand interactions at the binding pocket. These networks depict the amino acids involved in hydrogen bonding, van der Waals interactions, electrostatic interactions, or other types of interactions that furnish the stability of the ligand−protein complex (Figure 6).[37] In order to speculate the binding affinity of the most

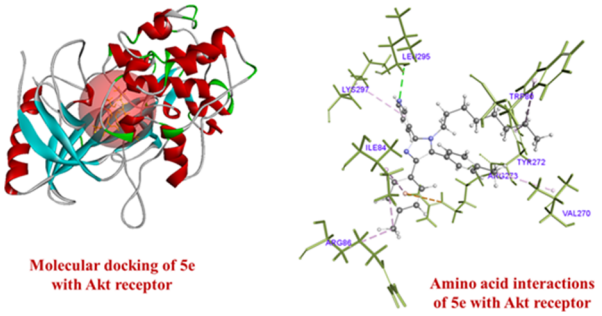

Figure 6. Molecular docking and amino acid interaction diagrams of **5e** with the Akt receptor.

potent synthesized compounds, namely, **5a**, **5d**, and **5e**, molecular docking simulations were conducted. These simulations involved docking the compounds into the active sites of proteins with PDB codes 4KZN, 7NH5, 5W9C, 3QYC, and 5GPG. These docking experiments provide insights into the potential binding modes and affinities of the compounds to the target proteins. Surface views of the **5e**−protein complex (Figure 7), the binding score (kcal/mol), and binding interactions of molecules **5a**, **5d**, and **5e** are reported (Supporting Information).

Binding affinity, represented by ΔG, is the stability of the binding interaction between a protein and its ligand. Higher docking scores indicate stronger binding affinity, and the results are shown in Table 2. The highest binding energy (−13.395 kcal/mol) was observed for the most active molecule, i.e., **5e**, which has an IC_{50} value of 39.19 ± 1.12 μM. The active compounds **5a** and **5d** also had binding energies of −9.211 and −12.885 kcal/mol, respectively, along with the molecular docking studies.

According to the Boiled egg diagram constructed by SWISS ADME, molecule **5a** is ideal for orally administered dosage forms as it has high GI absorption and blood−brain barrier

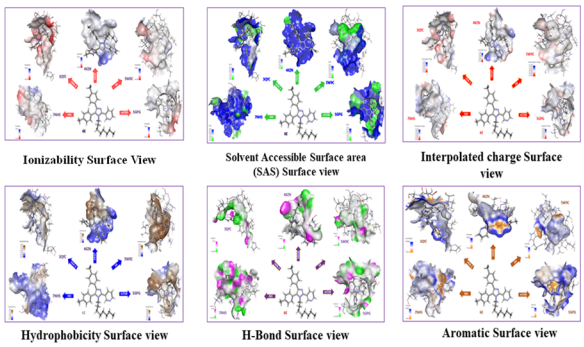

Figure 7. Amino acid interaction of lead molecule **5e** with various receptors in different surface views.

Table 2. DFT Analysis of Ligands

Code	HOMO energy (eV)	LUMO energy (eV)	Total energy (eV)	Binding energy (kcal/mol)	Dipole MAG (A m^2)
5a	−0.1813	−0.0674	−1004.81	−9.2114	1.1323
5d	−0.1777	−0.0647	−1277.38	−12.885	1.3974
5e	−0.1817	−0.0675	−1316.31	−13.395	1.0617

permeation. However, as observed from the bioavailability radar, molecule **5e** possesses the maximum bioavailability, followed by **5d** and the least by **5a** (Figure 8).

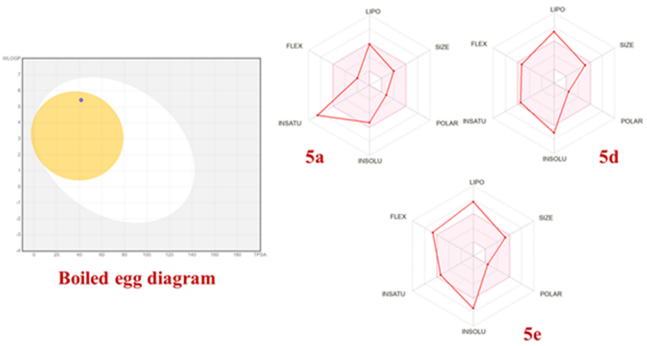

Figure 8. Boiled egg diagram and bioavailability radar of the active molecules.

2.4. Density Functional Theory. The potential performance of the ligands as inhibitors was evaluated by density functional theory (DFT) calculations. The DFT calculations of the selected compounds will facilitate the analysis of HOMO−LUMO energies, their differences, and other parameters to indicate the most potent candidates. The molecules with the least difference in HOMO−LUMO energy can be considered

https://doi.org/10.1021/acsomega.3c04384
ACS Omega 2023, 8, 40287−40298

promising. DFT calculations were employed in conjunction with molecular docking studies to better understand the ligands' potential as inhibitors. By utilizing DFT, the ligands' electronic structure, energetics, and other properties were computed and analyzed, providing valuable insights into their inhibitory capabilities. This integrated approach of DFT calculations and molecular docking allowed for a more detailed investigation and characterization of the ligands' binding interactions and potential as inhibitors. DFT calculations of the selected compounds will facilitate the analysis of HOMO−LUMO energies, their difference, and other parameters to indicate the most potent candidates. The molecules with the least difference in the HOMO−LUMO energy can be considered promising.

According to the DFT analysis, compound **5e** has the least difference between their HOMO and LUMO energy levels, while the other two molecules also show similar energy differences. The in silico toxicity predictions by TOPKAT account for the safe toxicity profile of **5e**, while the other two are likely to be toxic drugs.

3. STRUCTURE−ACTIVITY RELATIONSHIP ANALYSIS

To investigate the structure−activity relationship, the half-maximal inhibitory activity (IC_{50}) of the target compounds (**5a**, **5c**, **5d**, and **5e**) was evaluated against the T47D, MCF-7, MDA-MB-468, and BT474 cell lines. The IC_{50} values were determined by using SRB (sulforhodamine B) assays. This analysis aimed to identify and understand the correlation between the chemical structures of the compounds and their inhibitory activity against specific breast cancer cell lines. Two aspects were investigated in this study. The first aspect focused on assessing the cytotoxicity activity of the 3-(4,5-ditolyl-1H-imidazol-2-yl) pyridine scaffold. The aim was to determine the inherent cytotoxic potential of this scaffold against the target cells. The second aspect involved examining the effect of coupling different aliphatic substituents to the first position on the imidazole ring. This investigation aimed to evaluate how the introduction of various aliphatic groups impacted the cytotoxic activity of the compounds. By analyzing these two factors, the study aimed to elucidate the relationship between the chemical structure of the compounds and their cytotoxic effects. The results indicate that alkyl substitution in the first position of imidazole plays a central role in the anticancer effect of the compounds in the BT474 cell line. The alkyl chain (up to C8) can massively improve cytotoxicity against BT474 breast cancer cells (IC_{50} = 35.56 ± 1.02−45.82 ± 1.32 μM). It was found that when the alkyl chain length increases on the imidazole ring, the anticancer activity is reduced (IC_{50} = 50.08−100 μM). The in vitro anticancer activity evaluation found that the synthesized compounds **5a**, **5c**, **5d**, and **5e** showed good anticancer activity compared to **5f**−**5j**, which displayed moderate activities, as in Figure 9.

3.1. *In Silico* ADMET Analysis. Compared to conventional procedures, in silico predictions of the drug-likeness, physicochemical properties, or ADMET qualities have improved the possibility of identifying novel lead compounds in much less time. *In silico* studies were conducted to confirm the reliability of *in vitro* biological results. Several criteria were employed to assess the drug-likeness of the molecules, including Lipinski's rule of five, Veber rule, and consideration of oral bioavailability. Lipinski's rule of five evaluates parameters related to molecular weight, lipophilicity, hydrogen-bond donors, and hydrogen-bond acceptors. The Veber

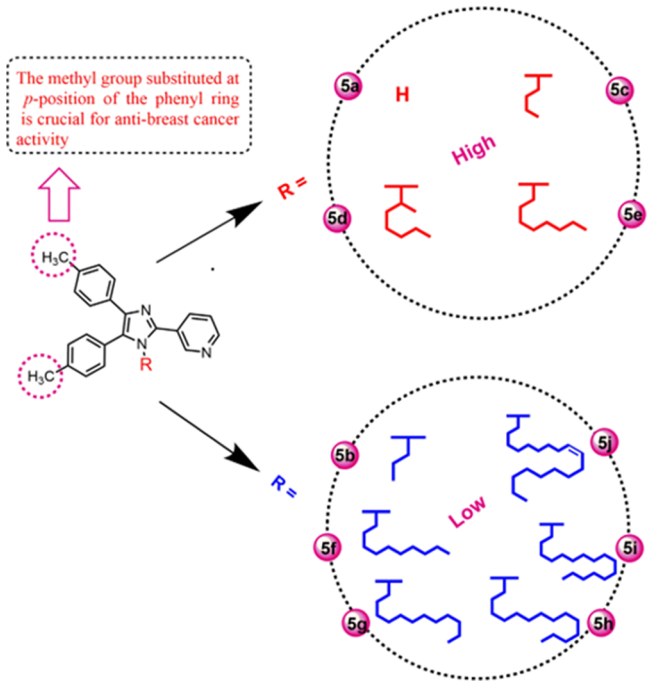

Figure 9. Structure−activity relationships of imidazole−pyridine scaffolds.

rule assesses the number of rotatable bonds in a molecule. These rules serve as guidelines for predicting the likelihood of a compound having favorable pharmacokinetic properties. In addition to these rules, the oral bioavailability of the candidate drugs was also considered. This parameter considers factors such as solubility, stability, permeability, and metabolic clearance, which are crucial for a drug to effectively absorb and reach systemic circulation when administered orally. By employing these evaluation criteria, the drug-likeness of the molecules was assessed, providing insights into their potential as candidates for further drug development. Analysis of the data demonstrated that four of the active compounds obey both rules. The effective drug pharmacokinetics of ADME was determined using Swiss-ADME predictors. Table 3 (Supporting Information) summarizes the physicochemical and pharmacokinetic properties.

4. CONCLUSIONS

In summary, this study focused on the design and synthesis of 3-(4,5-ditolyl-1H-imidazol-2-yl) pyridine scaffolds using a one-pot reaction. The synthesized compounds were then evaluated for their cytotoxicity against various breast cancer cell lines including MDA-MB-468, BT-474 (ER+, PR+, and HER2+), T-47D (ER+, PR+, and HER2−), and MCF-7 (ER+, PR+, and HER2−). Obviously, modifying the imidazole's N1 position alkyl chain increased its cytotoxic activity. These results showed the potential benefit of novel imidazole ring systems connected to alkyl chains (up to C8). The compound **5e** exhibited cytotoxic activity (IC_{50} = 39.19 ± 1.12 μM) against BT474 cells at 24 h. In silico toxicity prediction data revealed that the compound **5e** is noncarcinogenic and nonmutagenic in nature. The compound **5e** showed remarkable tumor volume reduction (50−66%) in the in vivo antibreast cancer assay. Regarding molecular modeling studies, compound **5e** showed high binding energy. According to the ADMET study, compound **5e** obeyed Lipinski's rule of five and has a flexible

https://doi.org/10.1021/acsomega.3c04384
ACS Omega 2023, 8, 40287−40298

Table 3. Physicochemical and Pharmacokinetic Parameters of Synthesized Compounds

	Lipinski's rule					Veber rule		Pharmacokinetics		Drug-likeness
Code	MW[a] < 500	M log P[b] ≤ 4.15	nHB[c] ≤ 10	nHB[d] ≤ 5	nRB[e] ≤ 10	TPSA[f] ≤ 140 Å^2	GI	BBB	log Kp −5.26 cm/s	Bioavailability score
5a	325.41	3.29	2	1	3	41.57	high	yes	−4.94	0.55
5b	367.49	3.92	2	0	5	30.71	high	no	−4.64	0.55
5c	381.15	4.13	2	0	6	30.71	low	no	−4.48	0.55
5d	423.59	4.72	2	0	8	30.71	low	no	−3.68	0.55
5e	437.62	4.91	2	0	10	30.71	low	no	−3.28	0.55
5f	465.67	5.29	2	0	12	30.71	low	no	−2.69	0.55
5g	493.73	5.66	2	0	14	30.71	low	no	−2.08	0.55
5h	521.78	6.02	2	0	16	30.71	low	no	−1.49	0.17
5i	549.83	6.37	2	0	18	30.71	low	no	−0.89	0.17
5j	575.87	6.65	2	0	19	30.71	low	no	−0.94	0.17

[a]Molecular weight. [b]Calculated lipophilicity. [c]Number of hydrogen bond acceptors. [d]Number of hydrogen bond donors. [e]Number of rotatable bonds. [f]Total polar surface area.

pharmacokinetic profile. The results showed that compound **5e** could potentially treat breast cancer.

5. EXPERIMENTAL SECTION

5.1. Chemistry. *5.1.1. Materials and Methods.* Chemicals were purchased from Sigma-Aldrich, Alfa-Aesar, Fluka, or Avra Synthesis Pvt., Ltd. and used directly from the source without further processing. In a Bruker AvanceTM 400 spectrometer, ^{1}H and ^{13}C NMR measurements were made in the deuterated solvent at 400.13 and 100.62 MHz, respectively. Purifications were performed using the designated eluents or flash chromatography on silica gel (60−120 mesh).

*5.1.2. General Procedure for the Synthesis of **5a**, **5c**−**5e**, and **5j**.* To initiate the reaction, a mixture consisting of 4,4′-dimethylbenzil (10 mmol), nicotinaldehyde (10 mmol), ammonium acetate (30 mmol), and primary amine (10 mmol) was dissolved in 10 mL of ethanol. Subsequently, a calculated catalytic amount of iodine was added to the mixture at a temperature of 78 °C. The reaction progress was monitored by using thin-layer chromatography (TLC). After the reaction completion, the mixture was subjected to product extraction. This process involved diluting the reaction mixture with a combination of water and ethyl acetate. The resulting solvent mixture was then separated, and the organic layer containing the desired compounds was isolated. To remove any residual moisture, the organic layer was treated with anhydrous sodium sulfate (Na_2SO_4). Next, the crude product obtained from the organic layer was further purified by using column chromatography. A column packed with silica gel (60−120 mesh size) was employed as the stationary phase, while a mixture of ethyl acetate and petroleum ether served as the eluent.

*5.1.2.1. 3-(4,5-Ditolyl-1H-imidazol-2-yl) Pyridine (**5a**).* Yellow powder. Obtained in 72% yield. m.p.: 171−172 °C, R_f = 0.24; (50% ethyl acetate in Pet. ether). FTIR (cm^{-1}): 3568 (N−H), 3064 (Ar−H), 2924 (−CH str in CH_3), 1519 (C═N), 1456 (C═C), 1021 (C−N), 816, 769 (Ar−H). ^{1}H NMR (400 MHz, $CDCl_3$) δ (ppm): 2.35 (s, 6H), 7.12−7.42 (m, 9H), 8.29−8.32 (t, 1H), 8.40−8.42 (d, 1H), 9.05 (d, 1H), 9.05 (d, 1H), 11.00 (s, 1H). ^{13}C NMR (101 MHz, $CDCl_3$) δ: 21.27, 123.92, 126.77, 127.80, 129.29, 133.41, 136.91, 142.75, 145.84, 148.83. MS (ESI +ve): 325.10 (M$^+$).

*5.1.2.2. 3-(1-Butyl-4,5-ditolyl-1H-imidazol-2-yl) Pyridine (**5c**).* Yellow powder. Obtained in 63% yield. m.p.: 72−73 °C. R_f = 0.38; (50% ethyl acetate in Pet. ether). FTIR (cm^{-1}): 2922 (−CH str in CH_3), 2856 (CH aliph.), 1592 (C═N), 1436 (C═C), 1026 (C−N), 806, 671 (Ar−H). ^{1}H NMR (400 MHz, $CDCl_3$) δ (ppm): 0.61- 0.65 (t, 3H), 0.95−1.04 (m, 2H), 1.31−1.38 (m, 2H), 2.28 (s, 3H), 2.44 (s, 3H), 3.86−3.90 (t, 2H), 7.01−7.03 (d, 2H), 7.28 (s, 4H), 7.39−7.45 (m, 3H), 8.05−8.08 (t, 1H), 8.66−8.68 (d, 1H), 8.94 (d, 1H). ^{13}C NMR (101 MHz, $CDCl_3$) δ 13.29, 19.48, 21.15, 21.45, 32.71, 44.64, 123.54, 126.64, 127.93, 128.11, 128.83, 129.82, 130.06, 130.83, 131.49, 135.98, 136.72, 138.39, 138.66, 144.09, 149.48, 149.58. MS (ESI +ve): 381.20 (M$^+$).

*5.1.2.3. 3-(1-(Beptan-2-yl)-4,5-ditolyl-1H-imidazol-2-yl) Pyridine (**5d**).* Brown, thick oil. Obtained in 68% yield. R_f = 0.25; (50% ethyl acetate in Pet. ether). FTIR (cm^{-1}): 2917 (−CH str in CH_3), 2849 (CH aliph.), 1542 (C═N), 1432 (C═C), 1091 (C−N), 808, 605 (Ar−H). ^{1}H NMR (400 MHz, $CDCl_3$) δ (ppm): 0.77−0.80 (t, 3H), 1.01−1.03 (t, 4H), 1.12−1.17 (m, 2H), 1.32−1.34 (d, 4H), 1.47−1.53 (m, 1H), 2.25 (s, 3H), 2.45 (s, 3H), 4.13−4.20 (m, 1H), 6.97−6.99 (d, 2H), 7.27−7.33 (m, 5H), 7.41−7.43 (m, 1H), 7.94−7.96 (t, 1H), 8.68−8.69 (d, 1H), 8.84 (d, 1H). ^{13}C NMR (101 MHz, $CDCl_3$) δ 13.96, 21.11, 21.46, 22.41, 26.04, 29.70, 31.22, 36.15, 53.97, 64.39, 123.26, 126.51, 128.75, 128.95, 129.53, 131.55, 131.82, 135.80, 137.62, 138.85, 149.79, 150.47. MS (ESI +ve): 423.20 (M$^+$).

*5.1.2.4. 3-(1-Octyl-4,5-ditolyl-1H-imidazol-2-yl) Pyridine (**5e**).* Brown, thick oil. Obtained in 61% yield. R_f = 0.25; (50% ethyl acetate in Pet. ether). FTIR (cm^{-1}): 3027 (Ar−H), 2922 (−CH str in CH_3), 2857 (CH aliph.), 1567 (C═N), 1458 (C═C), 1023 (C−N), 819, 711 (Ar−H). ^{1}H NMR (400 MHz, $CDCl_3$) δ (ppm): 0.85-.86 (t, 3H), 0.96−0.97 (d, 2H), 1.25−1.29 (m, 6H), 1.63 (s, 15H), 2.28 (s, 1H), 2.45 (s, 1H), 3.85−3.89 (t, 1H), 7.01−7.03 (d, 1H), 7.28 (s, 1H), 7.39−7.46 (m, 2H), 8.06−8.07 (d, 1H), 8.67−8.68 (d,1H), 8.93−8.94 (d, 1H). ^{13}C NMR (101 MHz, $CDCl_3$) δ: 14.06, 21.16, 21.44, 22.54, 26.15, 28.56, 28.79, 30.51, 31.60, 44.84, 123.54, 126.65, 127.88, 128.09, 128.84, 129.00, 129.83, 130.06, 130.83, 131.45, 136.01, 136.73, 138.68, 144.06, 149.46, 149.58. MS (ESI +ve): 437.25 (M$^+$). LCMS: 438.57 [M + H]$^+$. Retention time: 2.50 min, Purity = 99.81%.

*5.1.2.5. 3-(1-((E)-Octadec-10-enyl)-4,5-ditolyl-1H-imidazol-2-yl) Pyridine (**5j**).* Brown, thick oil. Obtained in 70% yield. R_f = 0.27; (50% ethyl acetate in Pet. ether). FTIR (cm^{-1}): 2969 (−CH str in CH_3), 2926, 2884 (CH aliph), 1603 (C═N), 1412 (C═C), 1119 (C−N), 816, 644 (Ar−H). ^{1}H NMR (400 MHz, $CDCl_3$) δ (ppm) 0.88−0.89 (d, 4H), 0.98 (s, 5H), 1.16 (s, 23H), 1.98−2.02 (m, 4H), 2.29 (s, 3H), 2.45 (s, 3H), 3.87−3.91 (t, 2H), 5.3−5.37 (q, 2H), 7.03−7.05

https://doi.org/10.1021/acsomega.3c04384
ACS Omega 2023, 8, 40287−40298

(d, 2H), 7.30 (s, 4H), 7.43−7.45 (d, 3H), 8.07−8.09 (d, 1H), 8.68 (d, 1H), 8.97 (s, 1H). ^{13}C NMR (101 MHz, $CDCl_3$) 12.82, 14.15, 21.17, 21.46, 22.70, 26.15, 27.16, 27.22, 28.59, 29.06, 29.33, 29.53, 29.65, 29.72, 29.76, 30.50, 31.91, 44.79, 123.50, 126.61, 127.93, 128.15, 128.82, 129.69, 129.81, 129.99, 130.33, 130.81, 131.54, 135.90, 136.33, 138.38, 138.61, 144.09, 149.49, 149.57. MS (ESI +ve): 575.15 (M^+).

5.1.3. General Procedure for the Synthesis of ***5b, 5f−5i.*** To carry out the reaction, a mixture containing 3-(4,5-ditolyl-1H-imidazol-2-yl) pyridine (0.33 mmol), K_2CO_3 (1.0 mmol), and acetonitrile (10 mL) was prepared. The corresponding alkyl bromide or alkyl iodide (1.0 mmol) was added to this mixture. The reaction mixture was then heated to 90 °C and stirred overnight until the reaction was complete. The reaction progress was monitored by using TLC. After the reaction was complete, the mixture was filtered to remove any solid impurities, and the solvent was removed under vacuum to obtain a residue. This residue was dissolved in ethyl acetate and washed with water to remove water-soluble impurities. The organic layer was separated, and any residual water was removed by drying it over anhydrous Na_2SO_4. The dried organic layer was then filtered to remove the drying agent. Column chromatography was performed using silica gel (60−120 mesh size) as the stationary phase to further purify the crude product. A mixture of ethyl acetate and petroleum ether was used as the eluent.

*5.1.3.1. 3-(1-Propyl-4,5-ditolyl-1H-imidazol-2-yl) Pyridine (****5b****).* Yellow powder. Obtained in 58% yield. m.p.: 112−113 °C. R_f = 0.20; (50% ethyl acetate in Pet. ether). FTIR (cm^{-1}): 3031 (Ar−H), 2923 (−CH str in CH_3), 2862 (CH aliph), 1574 (C═N), 1453 (C═C), 1022 (C−N), 813, 710 (Ar−H). ^{1}H NMR (400 MHz, $CDCl_3$) δ (ppm): 0.61−0.65 (t, 3H), 1.28−1.31 (s, 3H), 1.41−1.45 (m, 4H), 2.30 (s, 3H), 2.47 (s, 3H), 3.86−3.89 (t, 2H), 7.04−7.05 (d, 3H), 7.29−7.31 (m, 5H), 7.42−7.47 (m, 4H), 8.09−8.10 (d, 1H), 8.70 (d, 1H), 8.97 (s, 1H). ^{13}C NMR (101 MHz, $CDCl_3$) δ 10.87, 21.18, 21.47, 24.05, 46.45, 47.10, 123.57, 126.63, 127.94, 128.09, 128.83, 129.83, 130.07, 130.79, 131.46, 135.98, 136.75, 138.66, 144.11, 149.43, 149.55. MS (ESI +ve): 367.15 (M^+).

*5.1.3.2. 3-(1-Decyl-4,5-ditolyl-1H-imidazol-2-yl) Pyridine (****5f****).* Brown, thick oil. Obtained in 59% yield. R_f = 0.25; (50% ethyl acetate in Pet. ether). FTIR (cm^{-1}): 3018 (Ar−H), 2925 (−CH str in CH_3), 2857 (CH aliph.), 1616 (C═N), 1459 (C═C), 1028 (C−N), 823, 721 (Ar−H). ^{1}H NMR (400 MHz, $CDCl_3$) δ (ppm) 0.81-.084 (t, 3H), 0.92−0.99 (m, 3H), 1.15−1.22 (m, 2H), 1.25−1.29 (d, 2H), 1.41−1.42 (d, 1H), 1.71 (s, 11H), 2.28 (1H, 2H), 2.44 (s, 2H), 3.85−3.89 (t, 2H), 7.39−7.47 (d, 2H), 7.28 (s, 3H), 7.39−7.47 (m, 3H), 8.05−8.08 (t, 1H), 8.66−8.68 (d, 1H), 8.93−8.94 (d, 1H). ^{13}C NMR (101 MHz, $CDCl_3$) δ 14.05, 21.15, 21.44, 22.53, 26.15, 27.73, 28.01, 28.56, 28.79, 30.51, 31.60, 44.83, 123.53, 123.81, 123.89, 126.64, 128.13, 128.83, 129.81, 130.83, 136.71, 138.65, 143.43. MS (ESI +ve): 465.05(M^+).

*5.1.3.3. 3-(1-Dodecyl-4,5-ditolyl-1H-imidazol-2-yl) Pyridine (****5g****).* Brown, thick oil. Obtained in 64% yield. R_f = 0.28; (50% ethyl acetate in Pet. ether). FTIR (cm^{-1}): 3026 (Ar−H), 2923 (−CH str in CH_3), 2854 (CH aliph.), 1569 (C═N), 1462 (C═C), 1022 (C−N), 824, 717 (Ar−H). ^{1}H NMR (400 MHz, $CDCl_3$) δ (ppm) 0.89−0.9 (d, 5H), 1.28−1.31 (d, 29H), 2.30 (s, 2H), 2.47 (s, 1H), 3.87−3.91 (t, 1H), 7.04−7.05 (d, 1H), 7.29−7.31 (d, 2H),7.42−7.47 (m, 1H), 8.08−8.10 (d, 1H), 8.70 (d, 1H), 8.97 (s, 1H). ^{13}C NMR (101 MHz, $CDCl_3$): 14.15, 21.17, 21.46, 22.71, 26.16, 28.63, 29.16, 29.37, 29.42, 29.57, 29.66, 29.68, 30.52, 31.93, 44.83, 123.53, 126.61, 127.93, 128.12, 128.83, 129.81, 130.03, 130.82, 131.50, 135.95, 136.70, 138.37, 138.63, 144.08, 149.48, 149.57. MS (ESI +ve): 493.35 (M^+).

*5.1.3.4. 3-(1-Tetradecyl-4,5-ditolyl-1H-imidazol-2-yl) Pyridine (****5h****).* Brown, thick oil. Obtained in 58% yield. R_f = 0.27; (50% ethyl acetate in Pet. ether). FTIR (cm^{-1}): 3026 (Ar−H), 2923 (−CH str in CH_3), 2854 (CH aliph.), 1569 (C═N), 1462 (C═C), 1022 (C−N), 824, 717 (Ar−H). ^{1}H NMR (400 MHz, $CDCl_3$) δ (ppm) 0.90 (s, 4H), 0.98 (s, 5H), 1.27−1.30 (s, 21H), 2.30 (s, 3H), 2.47 (s, 3H), 3.88−3.91 (t, 2H), 7.04−7.05 (d, 2H), 7.31 (s, 4H), 7.47−7.44 (d, 3H), 8.08−8.10 (d, 1H), 8.70 (s, 1H), 8.97 (s, 1H). ^{13}C NMR (101 MHz, $CDCl_3$): 14.15, 21.17, 21.46, 22.71, 26.16, 28.63, 29.16, 29.37, 29.42, 29.57, 29.66, 29.68, 30.52, 31.93, 44.83, 123.53, 126.61, 127.93, 128.12, 128.83, 129.81, 130.03, 130.82, 131.50, 135.95, 136.70, 138.37, 138.63, 144.08, 149.48, 149.57. MS (ESI +ve): 521.05 (M^+).

*5.1.3.5. 3-(1-Hexadecyl-4,5-ditolyl-1H-imidazol-2-yl) Pyridine (****5i****).* Brown, thick oil. Obtained in 56% yield. R_f = 0.26; (50% ethyl acetate in Pet. ether). FTIR (cm^{-1}): 2919 (−CH str in CH_3), 2851 (CH aliph.), 1665 (C═N), 1455 (C═C), 1022 (C−N), 817, 715 (Ar−H). ^{1}H NMR (400 MHz, $CDCl_3$) δ (ppm) 0.90 (s, 4H), 0.98−1.04 (s, 7H), 1.27−1.43 (s, 23H), 2.30 (s, 3H), 2.47 (s, 3H), 3.88−3.91 (t, 2H), 7.04−7.05 (d, 2H), 7.31 (s, 4H), 7.42−7.44 (d, 1H), 8.08−8.10 (d, 1H), 8.70 (s, 1H), 8.97 (s, 1H). ^{13}C NMR (101 MHz, $CDCl_3$) 14.15, 21.17, 21.46, 21.73, 22.71, 26.17, 29.16, 29.38, 29.43, 29.57, 29.67, 29.71, 30.52, 31.89, 31.94, 45.18, 126.61, 127.93, 128.12, 128.82, 129.81, 130.02, 130.82, 131.50, 131.50, 133.19, 135.95, 136.70, 138.63, 144.08, 149.47, 149.57. MS (ESI +ve): 549.35 (M^+).

5.2. *In Vitro* and *In Vivo* Studies. *5.2.1. In Vitro Studies.* The breast cancer cell lines MCF-7, T47D, and MDA-MB-468 were obtained from the National Center for Cell Science, Pune, Maharashtra, India. The BT-474 cell line was provided by Dr. Annapoorni Rangarajan, Professor of Molecular Reproduction, Development, and Genetics at the Indian Institute of Science, Bangalore, India. The mouse fibroblast cell line L-929 was obtained from the ATCC culture. Dr. Prabhakar B.T from Shimoga, Karnataka, India's Kuvempu University's Post Graduate Department of Studies and Research in Biotechnology's Molecular Biomedicine Laboratory provided the EAC cells. As described in a previous study, cell lines were annually characterized and confirmed for their phenotypes and specific markers to ensure their authenticity and identity.[38] The breast cancer cell lines were cultured in DMEM (Dulbecco's modified Eagle's medium) supplemented with 4.5 g glucose/L, 10% FBS (fetal bovine serum), L-glutamine (2 mM final concentration), and antibiotics including penicillin (100 Units/mL), streptomycin (100 μg/mL), and ciprofloxacin-HCl (10 μg/mL).

5.2.1.1. Seeding of Cells into 96-Well Microtiter Plates. For the experimental setup, breast cancer cell lines and mouse fibroblast cell lines were plated in 96-well plates at a density of 10,000 cells per well, containing 100 μL of culture medium. The plates were then incubated in a CO_2 incubator (Forma SteriCycle, Thermo Scientific, Waltham, MA, USA) for approximately 30 h to allow the cells to reach a confluence of around 70%. Once the cells reached the desired confluence, they were tested with different compounds for 24 and 48 h. The treatments included a vehicle control using 0.1% DMSO (dimethyl sulfoxide) as the solvent, positive control using

https://doi.org/10.1021/acsomega.3c04384
ACS Omega 2023, 8, 40287−40298

Table 4. Details of *In Vivo* Study Providing the Number of Animals, Route of Administration, Dose, and Dosing Schedule

	Group − I	Group − II	Group − III	Group − IV	Group - V
Name	No tumor control	Tumor control	Test − I	Test − II	Positive control
Number of animals	3	9	6	6	4
Treatment agent	None	Vehicle	**5e**	**5e**	Cisplatin
Treatment agent concentration (mg/kg)	None	1% DMSO in saline	50 mg/Kg	250 mg/Kg	2.5 mg/Kg
Route of administration	No drug administration	Intraperitoneal	Intraperitoneal	Intraperitoneal	Intraperitoneal
Frequency of drug administration	No drug administration	Every alternate day	Every alternate day	Every alternate day	Every alternate day

cisplatin at a concentration of 100 μM, and the test compounds being evaluated. During the treatment period, the cells were maintained in the CO_2 incubator under appropriate conditions (e.g., temperature, humidity, and CO_2 concentration) to support their growth and viability.

5.2.1.2. Treatment with Compounds of Interest and Measurement of Cell Viability by SRB. Exponentially growing cells were treated with increasing concentrations (6.25−200 μM) of test scaffolds (**5a**−**5j**) for 24 and 48 h. The impact of these scaffolds on cell viability reduction was measured using the sulforhodamine-B (SRB) staining assay, as described by Skehan et al. in 1990.[39] Briefly, control and treated cells were fixed with 50% (w/v) trichloroacetic acid (TCA), followed by washing with water. The plates were then dried, and a 0.4% SRB solution was added to each well, allowing cell staining. Unbound SRB was washed with 1% acetic acid, and the bound SRB was solubilized with the Tris base solution. The optical density of the solubilized SRB was measured at 510 nm, and the percentage of cell viability was calculated by comparing the absorbance of the treated cells to that of the control cells.[40]

% Viability = 100 − [(OD of control − OD of sample)/OD of control)

5.2.2. In Vivo Studies. *In vivo* experiments (in mice) were carried out after receiving approval from the Institutional Animal Ethics Committee (IAEC; Approval #: JSS AHER/CPT/IAEC/090/2021) of the JSS Academy of Higher Education & Research. The Centre for Experimental Pharmacology and Toxicology (CEPT; Reg No: 261/PO/ReBi/S/2000/CPCSEA) has all the facilities required to conduct small animal studies. The animal protocol is depicted in Schematic #1. In brief, 4−6 week old female Swiss albino mice weighing about 22−25 g were randomly divided into five groups, as shown in Table 4. The number of animals in each group was decided based on prior studies.[41] Whereas Group-I has three animals, Groups-II, III, IV, and V have 9, 6,6, and 4 animals (Table 4). More animals were included in Group-II (tTumor control) due to the possibility of death after 2−3 weeks of study because of tumor burden. Only four animals were included in Group-V (positive control, cisplatin 2.5 mg/kg) as we have yet to observe many variations in tumor size or body weight during the experiment in our previous studies.

Animals were injected with 2×10^6 EAC cells/site intramuscularly, and tumors were allowed to grow for 6−8 days. The EAC model was chosen for evaluating the efficacy of **5e**, as this model is a well-accepted breast adenocarcinoma model to quickly evaluate the pharmacological actions of drugs. Ehrlich ascites carcinomas are characterized by high proliferation rates and rapid tumor development. Furthermore, unlike xenograft tumor studies, EAC studies are not expensive and do not require sophisticated facilities such as IVC cages, sterile feed, and water. Hence, this model was chosen to evaluate the in vivo efficacy of **5e**. When the tumors reached a size of about 50−75 mm^3, the treatment with each drug/vehicle control was initiated and continued until the tumors reached a size of about 3.0 cm^3. The treatment agents were administered intraperitoneally. The tumor size and body weight were measured just before the administration of each drug using a calibrated Vernier caliper (6" digital caliper with 0.1 mm accuracy, Perfect Sales India, Faridabad, Haryana, India) and a weighing scale (A123 Digital Compact Scale from ATOM, Zhejiang Junkaishunln Industries & Trade Co., Ltd., Zhejiang, China), as described by Bovilla.[41]

5.3. Molecular Modeling. *5.3.1. ADME and Toxicity Prediction.* The Swiss ADME tool, developed by the Swiss Institute of Bioinformatics and accessed through http://www.swissadme.ch/, and BIOVIA Discovery Studio was utilized for analyzing the pharmacokinetics, drug-likeness, and ADME profiles of the drugs. The SWISS ADME tool's bioavailability radar was employed to gain a general understanding of the suitability of the ligands for oral administration. Additionally, the Boiled egg construction provided insights into the ligands' potential for human gastrointestinal absorption (GIA) and blood−brain barrier (BBB) penetration. Furthermore, the QSTR (quantitative structure toxicity relationship) technique available in BIOVIA Discovery Studio's TOPKAT prediction module was utilized to predict the toxicity of the ligands.

5.3.2. Geometry Optimization. The preliminary structure modeling of the tested molecules **5a**, **5c**, **5d**, and **5e** was carried out using BIOVIA Draw V.21.1. Subsequently, the DMOl3 algorithm in Discovery Studio v21.1 was employed to identify the least energy structure through QM (quantum mechanics) energy calculations. For these calculations, molecules within a nonbond radius of 14 Å were considered the QM regions. The calculations were performed using the restricted spin method with an SCF (self-consistent field) density convergence of 10^{-7}. It was carried out using the B3LYP function, a generalized gradient approximation with gradient correction. Furthermore, DFT was employed to optimize the resulting geometries within the isovalue range of −0.05 to 0.1.

5.3.3. Molecular Docking. The docking into the ATP-binding site was conducted using the CDOCKER algorithm. This algorithm employs various sampling and scoring functions to identify the optimal binding pose of the ligand within the defined grid. Initially, the conformations of the ligand are determined and soft-core potentials are applied. This is followed by an MD (molecular dynamics) simulation-based annealing optimization technique to refine the ligand's conformation. Subsequently, a first-order minimization of the protein−ligand complex is performed, and the resulting complex is scored. A 2D and 3D visualization of the protein−ligand complex is employed to assess the interaction profile, providing insights into the specific interactions between the ligand and protein within the ATP-binding site.

5.4. Statistical Analysis. All in vitro studies were carried out in triplicate with at least three replicate wells in each experiment. The viability of compound-treated cells was

https://doi.org/10.1021/acsomega.3c04384
ACS Omega 2023, 8, 40287−40298

compared with that of vehicle-treated cells, and statistical significance was assessed by one-way ANOVA. In vivo studies were carried out by comparing the impact of the administration of the compound with that of vehicle-treated mice. One-way ANOVA was used to determine the significance among different groups. Results were considered significant if the P value is <0.05.

■ ASSOCIATED CONTENT

Supporting Information

The Supporting Information is available free of charge at https://pubs.acs.org/doi/10.1021/acsomega.3c04384.

Characterization details of compounds **5a−5j;** molecular docking studies by Biovia Discovery Studio; ADMET analysis; n-silico toxicity prediction and QSTR studies; DFT analysis of **5a, 5d, and 5e**; and amino acid interaction (PDF)

■ AUTHOR INFORMATION

Corresponding Authors

Carmelo Drago − *Institute of Biomolecular Chemistry, I-95126 Catania, Italy;* orcid.org/0000-0002-9924-179X; Email: carmelo.drago@cnr.it

Prasanna Ramani − *Dhanvanthri Laboratory, Department of Sciences, Amrita School of Physical Sciences and Center of Excellence in Advanced Materials & Green Technologies (CoE−AMGT), Amrita School of Engineering, Amrita Vishwa Vidyapeetham, Coimbatore 641112, India;* orcid.org/0000-0002-5236-7141; Email: r_prasanna1@cb.amrita.edu

Authors

Baladhandapani Aruchamy − *Dhanvanthri Laboratory, Department of Sciences, Amrita School of Physical Sciences and Center of Excellence in Advanced Materials & Green Technologies (CoE−AMGT), Amrita School of Engineering, Amrita Vishwa Vidyapeetham, Coimbatore 641112, India*

Mahadevaswamy G. Kuruburu − *Center of Excellence in Molecular Biology and Regenerative Medicine (CEMR, a DST-FIST Supported Center), Department of Biochemistry (a DST-FIST Supported Department), JSS Medical College, JSS Academy of Higher Education & Research, Mysore 570015 Karnataka, India*

Venugopal R. Bovilla − *Center of Excellence in Molecular Biology and Regenerative Medicine (CEMR, a DST-FIST Supported Center), Department of Biochemistry (a DST-FIST Supported Department), JSS Medical College, JSS Academy of Higher Education & Research, Mysore 570015 Karnataka, India*

SubbaRao V. Madhunapantula − *Center of Excellence in Molecular Biology and Regenerative Medicine (CEMR, a DST-FIST Supported Center), Department of Biochemistry (a DST-FIST Supported Department), JSS Medical College, JSS Academy of Higher Education & Research, Mysore 570015 Karnataka, India*

Sonu Benny − *Department of Pharmaceutical Chemistry, Amrita School of Pharmacy, Amrita Vishwa Vidyapeetham, Kochi, Kerala 682041, India*

Aneesh Thankappan Presanna − *Department of Pharmaceutical Chemistry, Amrita School of Pharmacy, Amrita Vishwa Vidyapeetham, Kochi, Kerala 682041, India;* orcid.org/0000-0003-0138-8249

Complete contact information is available at: https://pubs.acs.org/10.1021/acsomega.3c04384

Author Contributions

B.A.: Writing—original draft, formal analysis, investigation, data curation, and writing—review and editing. C.D.: Investigation, resources, writing—review and editing. P.R.: Conceptualization, supervision, project administration, writing—original draft, and writing—review and editing. T.P.A.: Software, writing—review and editing. S.B.: Formal analysis, data curation, and writing—review and editing. M.G.K. and Dr. V.R.B. have conducted the *in vitro* and *in vivo* experiments and compiled the data. The collected data were analyzed and interpreted by Dr. S.V.M. In addition, Dr. S.V.M. has written the methods and results of *in vitro* and *in vivo* experiments.

Notes

The authors declare no competing financial interest.

■ ACKNOWLEDGMENTS

The authors acknowledge the infrastructure support provided by the Department of Science and Technology to CEMR Laboratory (CR-FST-LS-1/2018/178) and to the Department of Biochemistry (SR/FST/LS-1-539/2012), the laboratory facilities provided by CEMR laboratory (DST-FIST-supported center), Department of Biochemistry (DST-FIST-supported department), Special Interest Group on Cancer Biology and Cancer Stem Cells (SIG-CBCSC), and JSS Academy of Higher Education and Research (Mysore, Karnataka, India). M.G.K. and V.R.B. are grateful to the Indian Council of Medical Research (ICMR) and the Government of India for the Senior Research Fellowship (SRF) award (Fellowship sanction No. 3/2/3/105/2019/NCD-III and 3/2/2/5/2018/online Onco Fship/NCD-III, respectively).

■ REFERENCES

(1) Giaquinto, A. N.; Sung, H.; Miller, K. D.; Kramer, J. L.; Newman, L. A.; Minihan, A.; Jemal, A.; Siegel, R. L. Breast Cancer Statistics, 2022, CA. *Cancer J. Clin.* **2022**, *72*, 524−541.

(2) Anwar, S. L.; Avanti, W. S.; Nugroho, A. C.; Choridah, L.; Dwianingsih, E. K.; Harahap, W. A.; Aryandono, T.; Wulaningsih, W. Risk factors of distant metastasis after surgery among different breast cancer subtypes: A hospital-based study in Indonesia, World. *J. Surg. Oncol.* **2020**, *18*, 1−16.

(3) Liu, T.; Song, S.; Wang, X.; Hao, J. Small-molecule inhibitors of breast cancer-related targets: Potential therapeutic agents for breast cancer. *Eur. J. Med. Chem.* **2021**, *210*, No. 112954.

(4) El-Gazzar, M. G. M.; Ghorab, M.M.; Amin, M.A.; Korany, M.; Khedr, M.A.; El-Gazzar, M. G.; Sakr, T.M. Computational, *in vitro* and radiation-based *in vivo* studies on acetamide quinazolinone derivatives as new proposed purine nucleoside phosphorylase inhibitors for breast cancer. *Eur. J. Med. Chem.* **2023**, *248*, No. 115087.

(5) Zeng, L.; Wu, Q.; Wang, T.; Li, L. P.; Zhao, X.; Chen, K.; Qian, J.; Yuan, L.; Xu, H.; Mei, W. J. Selective stabilization of multiple promoter G-quadruplex DNA by using 2-phenyl-1H-imidazole-based tanshinone IIA derivatives and their potential suppressing function in the metastatic breast cancer. *Bioorg. Chem.* **2021**, *106*, No. 104433.

(6) Berger, E.R.; Park, T.; Saridakis, A.; Golshan, M.; Greenup, R.A.; Ahuja, N. Immunotherapy treatment for triple negative breast cancer. *Pharmaceuticals* **2021**, *14*, 763.

(7) Chen, L.; Zhang, H.; Zheng, J.; Yu, S.; Du, J.; Yang, Y.; Liu, X. Thermo-sensitively and magnetically ordered mesoporous carbon nanospheres for targeted controlled drug release and hyperthermia application. *Mater. Sci. Eng. C* **2018**, *84*, 21−31.

(8) Yang, Y.; Zhang, H.; Wanyan, Y.; Liu, K.; Lv, T.; Li, M.; Chen, Y. Effect of Hydrophobicity on the Anticancer Activity of Fatty-Acyl-Conjugated CM4 in Breast Cancer Cells. *ACS Omega* **2020**, *5*, 21513−21523.
(9) Di Francesco, M.; Celia, C.; Cristiano, M. C.; D'Avanzo, N.; Ruozi, B.; Mircioiu, C.; Cosco, D.; Di Marzio, L.; Fresta, M. Doxorubicin Hydrochloride-Loaded Nonionic Surfactant Vesicles to Treat Metastatic and Non-Metastatic Breast Cancer. *ACS Omega* **2021**, *6*, 2973−2989.
(10) Sharma, D.; Kumar, S.; Narasimhan, B. Estrogen alpha receptor antagonists for the treatment of breast cancer: A review. *Chem. Cent. J.* **2018**, *12*, 1−32.
(11) Bai, X.; Ali, A.; Lv, Z.; Wang, N.; Zhao, X.; Hao, H.; Zhang, Y.; Rahman, F.U. Platinum complexes inhibit HER-2 enriched and triple-negative breast cancer cells metabolism to suppress growth, stemness and migration by targeting PKM/LDHA and CCND1/BCL2/ATG3 signaling pathways. *Eur. J. Med. Chem.* **2021**, *224*, No. 113689.
(12) Yang, J. L.; Ma, Y. H.; Li, Y. H.; Zhang, Y. P.; Tian, H. C.; Huang, Y. C.; Li, Y.; Chen, W.; Yang, L. J. Design, Synthesis, and Anticancer Activity of Novel Trimethoxyphenyl-Derived Chalcone-Benzimidazolium Salts. *ACS Omega* **2019**, *4*, 20381−20393.
(13) Alghamdi, S. S.; Suliman, R. S.; Almutairi, K.; Kahtani, K.; Aljatli, D. Imidazole as a promising medicinal scaffold: Current status and future direction. *Drug Des. Devel. Ther.* **2021**, *15*, 3289−3312.
(14) Gaba, M.; Mohan, C. Development of drugs based on imidazole and benzimidazole bioactive heterocycles: Recent advances and future directions. *Med. Chem. Res.* **2016**, *25*, 173−210, DOI: 10.1007/s00044-015-1495-5.
(15) Narasimhan, B.; Sharma, D.; Kumar, P. Biological importance of imidazole nucleus in the new millennium. *Med. Chem. Res.* **2011**, *20*, 1119−1140.
(16) Zhang, L.; Peng, X.; Damu, G.L. V; Geng, R.; Zhou, C. Comprehensive Review in Current Developments of Imidazole-Based Medicinal Chemistry. *Med. Res. Rev.* **2013**, 340−437.
(17) Ali, I.; Lone, M. N.; Aboul-Enein, H. Y. Imidazoles as potential anticancer agents. *Medchemcomm* **2017**, *8*, 1742−1773.
(18) Fang, Y.; Yuan, R.; Ge, W. Hui; Wang, Y. Jiang; Liu, G. Xiang; Li, M. Qi; Xu, J. Biao; Wan, Y.; Zhou, S. Liang; Han, X. Guang; Zhang, P.; Liu, J. Juan; Wu, H. Synthesis and biological evaluation of 1,2,4,5-tetrasubstituted imidazoles. *Res. Chem. Intermed.* **2017**, *43*, 4413−4421.
(19) Alghamdi, E. M.; Alamshany, Z. M.; El Hamd, M. A.; Taher, E. S.; Farrag El-Behairy, M.; Norcott, P. L.; Marzouk, A. A. Anticancer Activities of Tetrasubstituted Imidazole-Pyrimidine-Sulfonamide Hybrids as Inhibitors of EGFR Mutants, Chem. *Med. Chem.* **2023**, *18*, No. 202200641.
(20) Mohan, C. D.; Srinivasa, V.; Rangappa, S.; Mervin, L.; Mohan, S.; Paricharak, S.; Baday, S.; Li, F.; Shanmugam, M. K.; Chinnathambi, A.; Zayed, M. E.; Alharbi, S. A.; Bender, A.; Sethi, G.; Basappa; Rangappa, K. S. Trisubstituted-imidazoles induce apoptosis in human breast cancer cells by targeting the oncogenic PI3K/Akt/mTOR signaling pathway. *PLoS One* **2016**, *11*, 1−15.
(21) Liu, J.; Ming, B.; Gong, G. H.; Wang, D.; Bao, G. L.; Yu, L. J. Current research on anti-breast cancer synthetic compounds. *RSC Adv.* **2018**, *8*, 4386−4416.
(22) Sardar, A.; Ansari, A.; Gupta, S.; Sinha, S.; Pandey, S.; Rai, D.; Kumar, M.; Bhatta, R.S.; Trivedi, R.; Sashidhara, K. V. Design, synthesis and biological evaluation of new quinazolinone-benzopyran-indole hybrid compounds promoting osteogenesis through BMP2 upregulation. *Eur. J. Med. Chem.* **2022**, *244*, No. 114813.
(23) Upadhyay, A.; Chandrakar, P.; Gupta, S.; Parmar, N.; Singh, S. K.; Rashid, M.; Kushwaha, P.; Wahajuddin, M.; Sashidhara, K. V.; Kar, S. Synthesis, Biological Evaluation, Structure-Activity Relationship, and Mechanism of Action Studies of Quinoline-Metronidazole Derivatives Against Experimental Visceral Leishmaniasis. *J. Med. Chem.* **2019**, *62*, 5655−5671.
(24) Yu, B.; Qi, P. P.; Shi, X. J.; Huang, R.; Guo, H.; Zheng, Y. C.; Yu, D. Q.; Liu, H. M. Efficient synthesis of new antiproliferative steroidal hybrids using the molecular hybridization approach. *Eur. J. Med. Chem.* **2016**, *117*, 241−255.
(25) Mohamed, M. F. A.; Abuo-Rahma, G. E. D. A. Molecular targets and anticancer activity of quinoline-chalcone hybrids: Literature review. *RSC Adv.* **2020**, *10*, 31139−31155.
(26) Aruchamy, B.; Drago, C.; Russo, V.; Pitari, G. M.; Ramani, P.; Aneesh, T. P.; Benny, S.; Vishnu, V. R. Imidazole-pyridine hybrids as potent anti-cancer agents. *Eur. J. Pharm. Sci.* **2023**, *180*, No. 106323.
(27) Mantu, D.; Antoci, V.; Moldoveanu, C.; Zbancioc, G.; Mangalagiu, I. I. Hybrid imidazole (benzimidazole)/pyridine (quinoline) derivatives and evaluation of their anticancer and antimycobacterial activity. *J. Enzyme Inhib. Med. Chem.* **2016**, *31*, 96−103.
(28) Fan, Y.; Jin, X.; Huang, Z.; Yu, H.; Zeng, Z.; Feng, L.; Gao, T. Accepted Manuscript, 2018. DOI: 10.1016/j.ejmech.2018.03.016.-This.
(29) Siwach, A.; Verma, P. K. Synthesis and therapeutic potential of imidazole containing compounds. *BMC Chem.* **2021**, *15*, 1−69.
(30) Li, S.; Tan, Y.; Zhang, L.; Zhou, C. Comprehensive Insights into Medicinal Research on Imidazole-Based Supramolecular Complexes. *Pharmaceutics* **2023**, *15*, 1348 DOI: 10.3390/pharmaceutics15051348.
(31) Lončar, B.; Perin, N.; Mioč, M.; Boček, I.; Grgić, L.; Kralj, M.; Tomić, S.; Stojković, M. R.; Hranjec, M. Novel amino substituted tetracyclic imidazo[4,5-b]pyridine derivatives: Design, synthesis, antiproliferative activity and DNA/RNA binding study. *Eur. J. Med. Chem.* **2021**, *217*, No. 113342.
(32) Abonia, R.; Cortés, E.; Insuasty, B.; Quiroga, J.; Nogueras, M.; Cobo, J. Synthesis of novel 1,2,5-trisubstituted benzimidazoles as potential antitumor agents. *Eur. J. Med. Chem.* **2011**, *46*, 4062−4070.
(33) Nair, A. D.; Athira, C. K.; Manikandan, P.; Ramani, P. One-pot synthesis of modified 4-aryl-4H-chromenes and their preliminary anticancer studies. *J. Indian Chem. Soc.* **2019**, *96*, 19−22.
(34) Khan, K.; Siddiqui, Z. N. An Efficient Synthesis of Tri- and Tetrasubstituted Imidazoles from Benzils Using Functionalized Chitosan as Biodegradable Solid Acid Catalyst. *Ind. Eng. Chem. Res.* **2015**, *54* (26), 6611−6618.
(35) Benny, S.; Mishra, R.; Manojkumar, M.K.; Aneesh, T.P. From Warburg effect to Reverse Warburg effect; the new horizons of anticancer therapy. *Med. Hypotheses* **2020**, *144*, No. 110216.
(36) Rajendran, G.; Bhanu, D.; Aruchamy, B.; Ramani, P.; Pandurangan, N.; Bobba, K.N.; Oh, E.J.; Chung, H.Y.; Gangadaran, P.; Ahn, B.C. Chalcone: A Promising Bioactive Scaffold in Medicinal Chemistry. *Pharmaceuticals* **2022**, *15*, 1250.
(37) Revathidevi, S.; Munirajan, A. K. *Akt in Cancer: Mediator and More. Seminars in Cancer Biology*; Academic Press, December 1, 2019; pp. 80−91.
(38) Shen, C.; Gu, M.; Liang, D.; Miao, L.; Hu, L.; Zheng, C.; Chen, J. Establishment and characterization of three new human breast cancer cell lines derived from Chinese breast cancer tissues. *Cancer Cell Int.* **2009**, *9*, 3352−3364.
(39) Skehan, P.; Storeng, R.; Scudiero, D.; Monks, A.; Mcmahon, J.; Vistica, D.; Warren, J. T.; Bokesch, H.; Kenney, S.; Boyd, M. R. New colorimetric cytotoxicity assay for anticancer-drug screening. *J. Natl. Cancer Inst.* **1990**, *82*, 1107−1112.
(40) Kuruburu, M. G.; Bovilla, V. R.; Naaz, R.; Leihang, Z.; Madhunapantula, S. V. Variations in the Anticancer Activity of Free and Bound Phenolics of Finger Millet (Eleusine coracana (L) Gaertn; Variety KMR-301) Seeds. *Phytomed. Plus* **2022**, *2*, No. 100276.
(41) Bovilla, V. R.; Kuruburu, M. G.; Bettada, V. G.; Krishnamurthy, J.; Sukocheva, O. A.; Thimmulappa, R. K.; Shivananju, N. S.; Balakrishna, J. P.; Madhunapantula, S. V. Targeted inhibition of anti-inflammatory regulator nrf2 results in breast cancer retardation *in vitro* and *in vivo*. *Biomedicines* **2021**, *9*, 1−28.

https://doi.org/10.1021/acsomega.3c04384
ACS Omega 2023, 8, 40287−40298